Study of the phase transformations and equation of state of magnesium by synchrotron x-ray diffraction

Daniel Errandonea[1,3]**, Yue Meng**[1]**, Daniel Häusermann**[1] **and Takeyuki Uchida**[2]

[1] HPCAT, Carnegie Institution of Washington, Advanced Photon Source, Building 434E, Argonne National Laboratory, 9700 South Cass Avenue, Argonne, IL 60439, USA
[2] Consortium for Advanced Radiation Sources, University of Chicago, 5640 S Ellis Avenue, Chicago, IL 60637, USA

E-mail: derrandonea@hpcat.aps.anl.gov

Abstract

We studied the phase behaviour and the $P–V–T$ equation of state of Mg by *in situ* energy-dispersive x-ray diffraction in a multi-anvil apparatus in the pressure–temperature range up to 18.6 GPa and 1527 K. At high temperatures, an hcp to dhcp transition was found above 9.6 GPa, which differs from the hcp to bcc transformation predicted by theoretical calculations. At room temperature, the hcp phase remains stable within the pressure range of this study with an axial ratio, c/a, close to the ideal. The melting of Mg was determined at 2.2, 10 and 12 GPa; the detected melting temperatures are in good agreement with previous diamond anvil cell results. The $P–V–T$ equation of state determined based on the data of this study gives $B_0 = (36.8 \pm 3)$ GPa, $B_0' = 4.3 \pm 0.4$, $\alpha_0 = 25 \times 10^{-6}$ K^{-1}, $\partial\alpha/\partial T = (2.3 \pm 0.2) \times 10^{-7}$ K^{-2} and $\partial B_{0,T}/\partial T = (-2.08 \pm 0.09) \times 10^{-2}$ GPa K^{-1}.

1. Introduction

Magnesium (Mg) has received considerable attention in the past as an important alkaline-earth metal element existing in many compounds. Mg is a very compressible metal (bulk modulus of 35.4 GPa) [1] and at ambient conditions crystallizes in the hcp structure with an axial ratio, c/a, of 1.624 [2, 3], close to that of the ideal close-packing value ($c/a = 1.633$). The special interest in the high-pressure behaviour of Mg is due to the fact that the application of pressure (P) leads to an increased hybridization between s and p electrons [4] and induces an electron transfer from the sp bands to the initially empty 3d band [5–7]. These phenomena induce consequent changes in the electronic density of states and affect the structural stability of Mg. On the other hand, Mg is an ideal candidate for theoretical studies because of its simple

[3] Author to whom any correspondence should be addressed.

atomic configuration and because it is a nearly free-electron metal even under compression to about 100 GPa [8].

The pressure–temperature (P–T) phase diagram and the elastic properties of Mg have been widely investigated using theoretical methods [6, 9–11]. First-principles generalized pseudo-potential theory total-energy calculations [6] predicted an hcp to bcc transformation under high pressure at room temperature (RT). This transition was experimentally confirmed by energy-dispersive x-ray diffraction in a diamond anvil cell (DAC) and was placed at 50 ± 6 GPa [12]. In additional experimental high-pressure studies of Mg, the effects of pressure on its volume (V) and lattice parameters up to 30 GPa at RT [13, 14], its melting curve at high pressures up to 80 GPa [15–17], and the pressure behaviour of its transverse-optical phonon up to 50 GPa [18] were measured. The melting curve measured by Errandonea *et al* [17] using a laser-heated DAC shows a very good agreement with theoretical predictions [9].

The high P–T phase boundary between hcp and bcc has also been calculated [9]. This boundary, according to that calculation [9], is highly temperature dependent and has a negative slope. It ends at a triple point on the melting curve near 4 GPa and 1200 K as shown in the P–T phase diagram of Mg illustrated in figure 1. Despite the intensive theoretical study of the high P–T phase diagram of Mg, so far only its melting curve has been measured [15–17] under high P–T conditions. In particular, the predicted hcp–bcc phase boundary has never been experimentally investigated. Furthermore, the melting data for Mg do not show any indication of the existence of a triple point [17] (i.e. no sharp change in the melting slope is observed as shown in figure 1), casting some doubts on the correctness of the theoretical predicted hcp–bcc boundary line [9]. In addition, the observed broadening and splitting of the E_{2g} Raman mode of Mg at RT above 10 GPa [18] and the indications of the possible existence of a dhcp phase found early on by Perez-Albuerne *et al* at RT above 5 GPa [14] indicate that the known crystal-structure sequence might be in error.

The facts described above emphasize the need for a detailed experimental study of the P–T phase diagram of Mg. In the present work we present an energy-dispersive synchrotron powder x-ray diffraction investigation of Mg in the P–T range up to 18.6 GPa and 1527 K. No evidence supporting the occurrence of a hcp $\rightarrow$ bcc transition is observed. On the contrary, at pressures exceeding 7.5 GPa we observed a transition from hcp to dhcp at high temperature. The present results allow us to characterize the stability field of hcp Mg by the location of the hcp–dhcp boundary. The experimental P–V–T data set is also used to determine a high-temperature equation of state (EOS).

2. Methods and materials

High P–T energy-dispersive x-ray powder diffraction (EDXRD) experiments were performed in a 250 ton multi-anvil apparatus installed at the GSECARS 13-BM-D beam line at the APS, using a double-stage split-cylinder 'T-cup' assembly and pyrophyllite octahedral pressure cells [19]. With this set-up, experiments on millimetre-sized cylindrical samples with excellent T and P stability and uniformity can be carried out up to 20 GPa and 2000 K. In this study, diffraction patterns were collected in the energy range from 20 to 130 keV with an incident x-ray beam size of 100 μm $\times$ 300 μm. A Ge solid-state detector at a fixed diffraction angle of 5.38° was used to detect the diffracted x-rays. High temperature was generated by resistance heating of two TiC/diamond discs located at both ends of the sample-cell assembly. Mg samples were isolated from the heater by hexagonal boron nitride (BN) discs (see figure 2). Temperature was determined based on the measured electromotive force (emf) of a $W_{0.94}Re_{0.06}$–$W_{0.75}Re_{0.25}$ thermocouple (type D). No corrections for pressure effects on the thermocouple emf were made because, as emphasized by previous workers [20–22], there is no universal correction factor
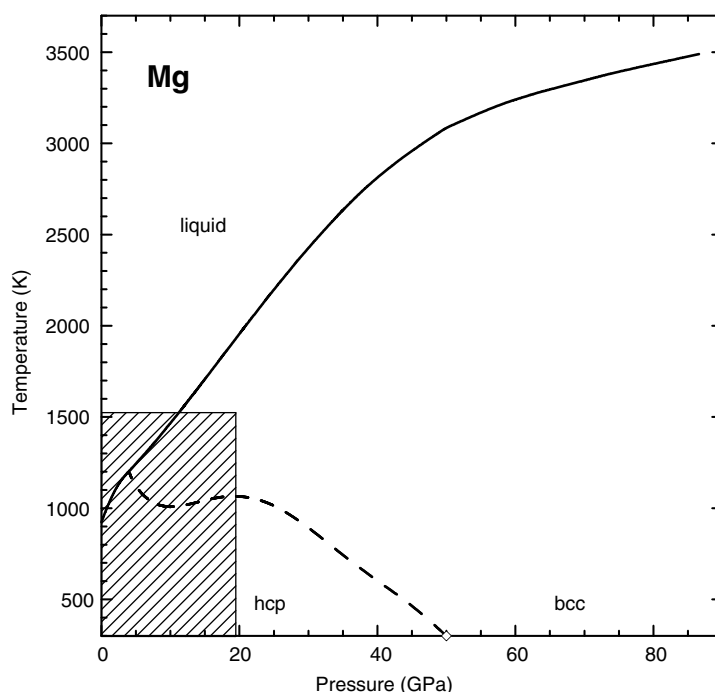
Figure 1. P–T phase diagram of Mg according to literature data. Melting curve [17] (full curve), calculated hcp–bcc phase boundary [9] (dashed curve) and experimentally determined RT hcp → bcc transition [12] ($\Diamond$). The hatched area represents the P–T region studied here.

that may be applied to correct the effects of pressure on the thermocouple emf. However, the maximum temperature uncertainty in the present P–T range can be estimated to be less than 30 K [22]. On the other hand, the maximum temperature fluctuation observed during the experiments was only about 5 K at 1500 K.

The experimental assembly is shown in figure 2. The thermocouple is located at the centre, isolated from the sample by a mixture of sodium chloride (NaCl) and BN powders. One half of the pressure cell is loaded with high-purity (99.8%) Mg powder obtained from the Johnson Matthey Company and stored under vacuum to avoid oxidation. The other half of the pressure cell was loaded with a mixture of Mg and gold (Au) powders with a weight ratio of 10:1. Pressures were calibrated using the diffraction lines of Au [23]. The diffraction lines of NaCl were also used to double-check the pressures based on Decker's EOS [24]. A comparison of the two calibrations showed that the pressures based upon Au and NaCl agree within ±0.1 GPa, suggesting that there is no observable effect of deviatory stress. This is consistent with the fact that Mg (bulk modulus 35.4 [1]) is a much softer material than Au (bulk modulus 166.7 [23]). On the other hand, the error introduced when determining the pressure through the P–V–T EOS of either Au or NaCl because of the temperature uncertainty is negligible compared with the pressure difference between both calibrations. Therefore the sample pressure can be considered accurate to within ±0.1 GPa. Additionally, high-temperature annealing was also used to reduce the non-hydrostatic stress in measurements at high pressures.

The pressure-induced transformations were examined in three different experimental runs. The different experimental paths used for studying the P–T behaviour of Mg are shown in figure 3. Diffraction patterns of Mg, the mixture of Mg and Au, and NaCl were collected at each P–T point. Indexing, structure solution and refinements were carried out using XRDA [25]
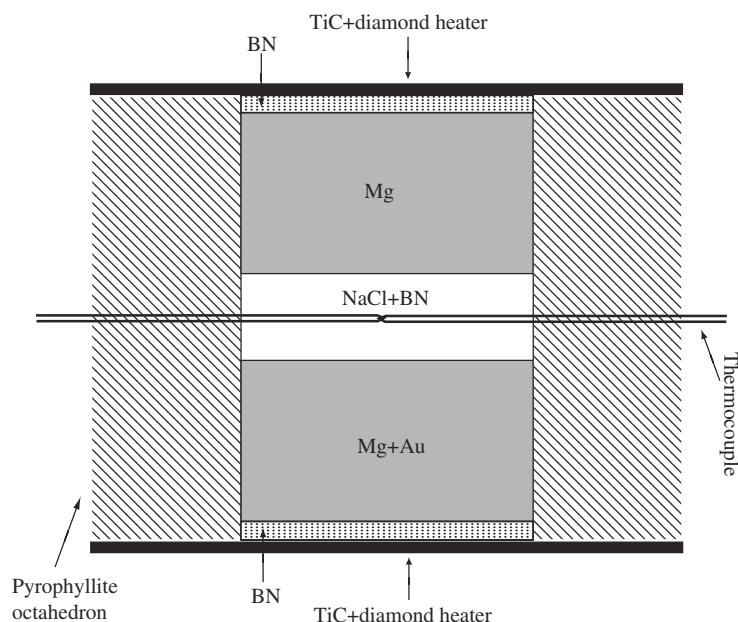
Figure 2. Schematic view of the high-pressure cell used to perform the present high P–T x-ray diffraction studies of Mg.

and GSAS [26] programs. A typical diffraction spectrum contains three phases: Mg, Au and NaCl, with at least six diffraction peaks associated with Mg. BN diffraction lines were never observed as a consequence of its low atomic number and its low concentration in the NaCl:BN mixture. To obtain the lattice parameters of each phase a LeBail refinement [27] was performed.

3. Results and discussion

3.1. Phase transformation at high P–T

Within the P–T range of this study, we did not find any evidence of the existence of a bcc phase at high temperature as predicted by previous theoretical calculations [9]. At three different pressures (2.3, 10.1 and 11.9 GPa) the samples were heated up to temperatures where the Mg peaks disappeared. Even in these runs, we did not find any indication of the existence of the bcc phase. The disappearance of the Mg diffraction peaks (see trace (e) in figure 4) together with the observed increase of the background is probably related to the onset of melting. The melting points obtained in this way agree well, within experimental error, with previous results (see figure 3). It is important to note that above 1350 K, an additional weak peak was observed that may be explained by the MgO(111) diffraction line and could be attributed to the formation of a small amount of MgO. Partial oxidation under high P–T conditions has been reported previously in other alkaline-earth metals [28], not affecting the results on the phase diagram when the oxide peaks are well identified.

In contrast to the predicted hcp to bcc transformation, we observed the splitting of the 002 peak of hcp Mg, as well as two new peaks between the 101 and the 102 peaks and between the 102 and the 110 peaks (see traces (d) and (c) in figure 4). Figure 4 shows energy dispersive
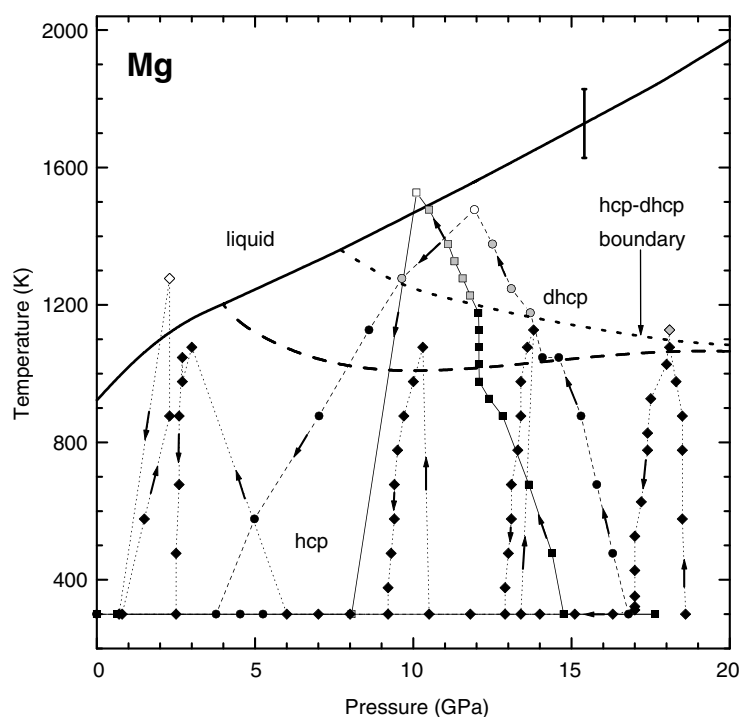
Figure 3. $P-T$ phase diagram of Mg at pressures below 20 GPa together with the experimental $P-T$ paths. The arrows show directions of the $P-T$ path. Diamonds, circles and squares represent the three runs performed. Full symbols indicate the stability region of the hcp phase, shaded symbols indicate the stability region of the dhcp phase and open symbols indicate the observation of melting. Previous melting data are [17] (full curve) shown with a typical error bar, calculated hcp–bcc boundary [9] (long-dashed curve), and present hcp–dhcp boundary (short-dashed curve).

x-ray spectra recorded under different $P-T$ conditions in one of the experimental runs. In this run, we increased P up to 14.75 GPa at RT, and then the temperature was increased at a constant hydraulic ram load. At RT and 977 K (see traces (a)–(c) in figure 4), the diffraction patterns of Mg can be indexed by the hcp structure. As T is increased to 1377 K the three new peaks mentioned above appeared (see trace (d) in figure 4). Analysis of the diffraction pattern shows that the locations of the new peaks are precisely what one would expect for the 101, 103 and 105 peaks of the dhcp structure (ABACABAC... stacking instead of ABABABAB... stacking of the hcp structure)[4]. Table 1 compares the observed and calculated lattice spacings (d spacings) for Mg at 11.1 GPa and 1377 K, showing a good fit to the dhcp lattice with a mean error in d spacings of less than 0.8%. In table 1, we also listed the calculated diffraction lines for an equivalent hcp structure for comparison. Figure 3 shows all the $P-T$ points where we observed the dhcp diffraction lines. With these data a hcp–dhcp boundary can be drawn, intercepting the melting curve around 7.5 GPa and 1350 K. This boundary line is illustrated in figure 3 (short-dashed curve) together with the theoretically predicted hcp–bcc boundary line (long-dashed curve) and the experimental melting curve (full curve).

[4] The dhcp structure has the same space group as the hcp structure ($P6_3/mmc$), but because of the different stacking order of hexagonal planes the dhcp structure has $z = 4$ instead of $z = 2$ (two atoms at b positions and two at f positions). As its unit cell is exactly double that in the hcp structure, the dhcp structure gives additional Bragg peaks. Therefore many correspondences are expected between the reflections of both structures, as shown in table 1.
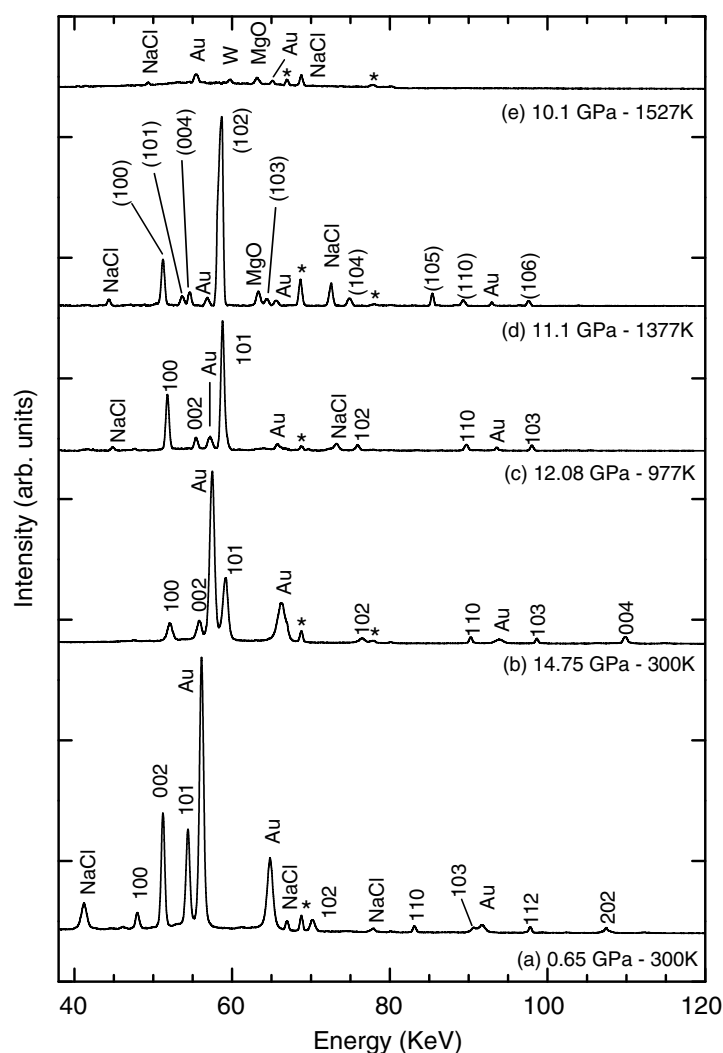
Figure 4. Mg x-ray diffraction pattern obtained at five different $P-T$ conditions in one experimental run. Miller indices corresponding to the hcp Mg structure are indicated. Au diffraction lines are shown. NaCl, W (from the thermocouple), MgO and fluorescence ($*$) peaks are also labelled when observed. The upper trace illustrates the melting of Mg. The second trace shows the onset of dhcp peaks. These peaks are indexed between brackets. The background was subtracted.

In order to get some insight into the mechanism involved in the proposed hcp–dhcp transformation, it is important to note that a single stacking fault transforms the hcp structure into the dhcp structure [29]. In addition, it is well known that in close-packed metals, such as Mg, stacking faults are formed with relative ease, contributing to the ductile nature of these metals [30]. Thus, it is reasonable to expect that at high temperature a thermal fluctuation will create stacking faults transforming the hcp structure into the dhcp structure. On the other hand, no difference in atomic volume between the hcp and dhcp structures was observed. This is because the two structures represent polytypes of the same structure with different stacking sequences. A similar hcp $\rightarrow$ dhcp transformation has been observed in iron at high temperature near 40 GPa [31, 32] and in other close-packed metals under compression [31, 33, 34].

Table 1. Observed and calculated lattice spacings (d) for Mg at 11.1 GPa and 1377 K. Calculations are done for a dhcp lattice with $a = 3.075$ Å and $c = 9.974$ Å and for an equivalent hcp lattice ($c = 4.987$ Å). The errors of the observed d values are given in brackets.

	dhcp		hcp	
d_{obs} (Å)	d_{calc} (Å)	hkl	d_{calc} (Å)	hkl
2.674(4)	2.663	100	2.663	100
2.552(4)	2.573	101	—	—
2.509(3)	2.493	004	2.493	002
2.340(2)	2.349	102	2.349	101
2.093(3)	2.078	103	—	—
1.830(1)	1.820	104	1.820	102
1.604(1)	1.597	105	—	—
1.534(3)	1.537	110	1.537	110
1.400(1)	1.410	106	1.410	103

Indications of the existence of the dhcp phase in Mg were previously reported at high pressure and RT [14, 18]. In the present study, the dhcp phase was only found at high temperatures, the hcp–dhcp boundary having a negative slope (see short-dashed curve in figure 3). After melting and quenching one of the runs from 10.1 GPa and 1527 K to 8.05 GPa and 300 K the diffraction lines associated with the appearance of the dhcp phase were also observed at RT (see table 2). However, when releasing compression to ambient pressure, these lines disappeared, suggesting that the dhcp is a metastable phase even at pressures as low as 10 GPa. Two possible scenarios are then compatible with our results; either at sufficiently high P the hcp–dhcp transition occurs at ambient temperature before the stability of the bcc phase is reached or an hcp–dhcp–bcc critical point exists in the solid at a temperature below melting.

At this point it is worthwhile commenting upon two facts that could probably have conspired to hide the existence of an hcp $\rightarrow$ dhcp transformation in previous works. The first one is that in the theoretical calculations of the P–T phase diagram of Mg, only the bcc, fcc and hcp structures were considered as possible stable phases [5, 9] and therefore the stability of the dhcp phase could not be predicted. The second one is that in the experiment that reported a direct hcp $\rightarrow$ bcc phase transition at 50 ± 6 GPa and RT [12] only three diffraction lines belonging to both the hcp and the bcc phases were observed and the signal-to-background ratio was quite low. In particular, in [12] the 002 diffraction peak of the hcp phase was not observed, possibly due to preferred orientations caused by uniaxial stresses in the DAC [35]. Since one of the inherent dhcp peaks reported here arises from the splitting of the 002 reflex of the hcp phase (see figure 4), the absence of this diffraction line, added to the fact that the other two inherent dhcp peaks observed here are weak enough not to be seen with the low signal to noise ratio of the experiment reported in [12], may have caused misleading identification of the structural sequence of Mg.

Before closing the discussion about the phase diagram of Mg, one should also notice that the present results might explain why the melting data fail to show any change in the melting slope around 4 GPa [17] as expected from the predicted hcp–bcc–liquid triple point. In fact, the intersection of the melting curve with a solid–solid boundary line between two close-packed structures (instead of an hcp–bcc boundary line), as reported here, should lead to a smooth behaviour of the melting curve [36–39], like that previously measured [17]. Obviously, further experimental and theoretical work is necessary to verify our arguments. In particular, new structural studies to pressures higher than 50 GPa in the temperature range accessible through

Table 2. Experimental $P-V-T$ data points obtained for Mg in the three experimental runs. Unit cell parameters and axial ratios are also listed; their estimated error is smaller than 0.1%. The phase observed at each point is indicated in the last column. The data are given following the collection sequence.

Pressure (GPa)	Temperature (K)	a (Å)	c (Å)	c/a^a	Volume (cm^3 mol^{-1})	Phase
0.65	300	3.176	5.152	1.622	13.55	hcp
17.65	300	2.922	4.726	1.617	10.52	hcp
14.75	300	2.959	4.783	1.616	10.92	hcp
14.38	477	2.974	4.815	1.619	11.10	hcp
13.65	677	2.989	4.842	1.620	11.28	hcp
12.82	877	2.997	4.837	1.614	11.33	hcp
12.4	927	2.991	4.851	1.622	11.32	hcp
12.4	927	2.999	4.828	1.610	11.32	hcp
12.08	977	3.001	4.757	1.617	11.40	hcp
12.07	1027	3.041	4.917	1.617	11.86	hcp
12.07	1077	3.043	4.923	1.618	11.89	hcp
12.07	1077	3.040	4.922	1.619	11.86	hcp
12.07	1127	3.046	4.925	1.617	11.91	hcp
12.07	1127	3.051	4.930	1.616	11.97	hcp
12.06	1177	3.041	4.920	1.618	11.86	hcp
11.8	1227	3.059	9.892	1.617	12.07	dhcp
11.8	1227	3.059	9.868	1.613	12.04	dhcp
11.56	1277	3.058	9.882	1.616	12.05	dhcp
11.30	1327	3.067	9.954	1.623	12.21	dhcp
11.30	1327	3.062	9.938	1.623	12.15	dhcp
11.1	1377	3.075	9.974	1.622	12.30	dhcp
10.7	1427	3.088	10.004	1.620	12.44	dhcp
10.5	1477	3.091	10.020	1.621	12.48	dhcp
10.1	1527					liquid
8.05	300	3.036	9.926	1.619	11.81	dhcp
0	300	3.202	5.208	1.626	13.92	hcp
0	300	3.204	5.213	1.627	13.95	hcp
0	300	3.214	5.217	1.623	14.05	hcp
4.53	300	3.094	5.001	1.616	12.48	hcp
5.25	300	3.087	5.006	1.621	12.44	hcp
16.8	300	2.927	4.730	1.616	10.57	hcp
16.3	477	2.939	4.746	1.615	10.69	hcp
15.8	677	2.959	4.769	1.612	10.89	hcp
15.3	877	2.967	4.797	1.617	11.01	hcp
14.6	1047	2.969	4.814	1.622	10.73	hcp
14.08	1047	2.917	4.757	1.631	10.55	hcp
13.7	1177	2.976	9.630	1.618	11.12	dhcp
13.1	1247	3.010	9.744	1.619	11.51	dhcp
12.5	1377	3.013	9.714	1.612	11.49	dhcp
11.93	1477					liquid
9.64	1277	3.079	9.984	1.621	12.34	dhcp
8.6	1127	3.124	5.056	1.618	12.87	hcp
7.02	877	3.142	5.072	1.614	13.06	hcp
4.98	300	3.110	5.045	1.622	12.73	hcp
3.77	300	3.069	4.964	1.617	12.19	hcp
0	300	3.189	5.185	1.626	13.75	hcp
18.6	300	2.933	4.736	1.615	10.62	hcp
18.5	577	2.931	4.746	1.619	10.66	hcp

Table 2. (Continued.)

Pressure (GPa)	Temperature (K)	a (Å)	c (Å)	c/a[a]	Volume (cm³ mol⁻¹)	Phase
18.5	777	2.938	4.746	1.618	10.70	hcp
18.5	877	2.943	4.761	1.618	10.75	hcp
18.3	977	2.947	4.771	1.619	10.81	hcp
18.1	1077	2.951	4.780	1.620	10.83	hcp
18.1	1127	2.953	9.564	1.619	10.85	dhcp
18	1027	2.951	4.783	1.621	10.87	hcp
17.5	927	2.949	4.778	1.620	10.86	hcp
17.4	827	2.947	4.773	1.619	10.84	hcp
17.4	777	2.947	4.770	1.619	10.81	hcp
17.2	627	2.944	4.768	1.620	10.80	hcp
17	527	2.944	4.766	1.619	10.78	hcp
17	427	2.943	4.764	1.619	10.77	hcp
17	352	2.942	4.765	1.620	10.76	hcp
17	322	2.943	4.764	1.619	10.75	hcp
17	312	2.941	4.762	1.619	10.75	hcp
16.3	300	2.951	4.774	1.618	10.74	hcp
15.1	300	2.961	2.961	1.616	10.84	hcp
14	300	2.970	4.810	1.619	10.96	hcp
13.4	300	2.971	4.786	1.616	11.07	hcp
13.8	1127	2.996	4.856	1.621	11.09	hcp
13.6	1077	3.002	4.862	1.620	11.37	hcp
13.4	977	3.018	4.860	1.617	11.43	hcp
13.4	877	2.993	4.851	1.617	11.42	hcp
13.3	777	2.998	4.848	1.617	11.38	hcp
13.1	677	2.996	4.840	1.617	11.36	hcp
13.1	577	2.993	4.840	1.617	11.31	hcp
13	477	2.992	4.837	1.617	11.31	hcp
12.9	377	2.990	4.836	1.617	11.29	hcp
12.9	300	2.990	4.835	1.617	11.27	hcp
11.8	300	3.001	4.853	1.617	11.27	hcp
10.5	300	3.018	4.876	1.616	11.39	hcp
10.3	1077	3.053	4.948	1.620	11.58	hcp
10	977	3.056	4.943	1.618	12.03	hcp
9.7	877	3.051	4.933	1.617	12.01	hcp
9.5	777	3.050	4.924	1.614	11.98	hcp
9.4	677	3.048	4.924	1.616	11.94	hcp
9.3	577	3.045	4.920	1.616	11.93	hcp
9.2	477	3.046	4.925	1.617	11.90	hcp
9.2	377	3.040	4.898	1.611	11.91	hcp
9.2	300	3.040	4.910	1.615	11.80	hcp
8	300	3.056	4.940	1.617	11.84	hcp
7	300	3.072	4.967	1.617	12.03	hcp
6	300	3.090	4.988	1.614	12.22	hcp
3	1077	3.197	5.188	1.623	12.41	hcp
2.7	977	3.195	5.187	1.623	13.83	hcp
2.7	1047	3.195	5.189	1.624	13.81	hcp
2.6	877	3.196	5.191	1.624	13.81	hcp
2.6	677	3.199	5.198	1.625	13.84	hcp
2.5	477	3.191	5.177	1.622	13.89	hcp
2.5	300	3.121	5.054	1.621	13.75	hcp
0.8	300	3.199	5.186	1.621	12.84	hcp

Table 2. (Continued.)

Pressure (GPa)	Temperature (K)	a (Å)	c (Å)	c/a[a]	Volume (cm^3 mol^{-1})	Phase
1.5	577	3.199	5.191	1.622	13.84	hcp
2.3	877	3.193	5.184	1.624	13.85	hcp
2.3	1277					liquid
0.7	300	3.201	5.188	1.621	13.78	hcp

[a] We list $c/2a$ for the dhcp structure instead of c/a to allow direct comparison with the hcp structure.

external-heated DACs, taking advantage of high-brilliance third-generation synchrotrons and angle-dispersive techniques, are needed to unambiguously solve the P–T phase diagram of Mg and verify whether the known RT crystal structure sequence is in error.

3.2. P–V–T equation of state

The RT pressure–volume (P–V) data from this study are plotted in figure 5 together with data reported in previous experiments [13, 14]. A Birch–Murnaghan third-order EOS [40] fitted to all data shown in figure 5 yields the following parameters for the RT bulk modulus (B_0), its pressure derivative (B_0') and the atomic volume (V_0) respectively: $B_0 = (36.8 \pm 3)$ GPa, $B_0' = 4.3 \pm 0.4$, and $V_0 = (13.88 \pm 0.09)$ cm^3 mol^{-1}. These parameters are in good agreement with those reported previously [3, 13, 14, 41]. The calculated volume at 50 GPa based on the present EOS agrees with the volume reported in [12] (see figure 5).

The variation of the axial ratio, c/a, at RT as a function of pressure is shown in figure 6. The c/a ratio is nearly independent of pressure with an extremely small negative slope. Our data can be fitted to the following equation:

$$c/a = 1.624 - 9.3(6) \times 10^{-4}P + 2.5(5) \times 10^{-5}P^2, \tag{1}$$

where P is in GPa and $P < 18.6$ GPa. This behaviour is not consistent with previous studies [13, 14] as shown in figure 6. However, we want to point out here that in [13] and [14] only three diffraction peaks were used to calculate the unit cell parameters and among them only the 101 line involves c. On the other hand, there are several facts that support our results. A similar axial-ratio pressure dependence to that we found in Mg was also observed in beryllium [42], which is another light alkaline-earth metal with nearly free electron behaviour. In addition, in zinc, another divalent hcp metal, an anomaly on the c/a was observed only in experiments carried out under highly non-hydrostatic conditions [43]. And finally, according to full-potential calculations [4] in Mg, the electrostatic part of the total energy dominates over the band energy. Therefore, any pressure-induced change of the s–p hybridization is not structure determining and consequently c/a is expected to stay roughly constant as we observed.

We have used all the P–V–T data from this study (see table 2), previous P–V data at RT [13, 14] and previous V–T data at ambient pressure [44] to obtain a P–V–T EOS for Mg. Since there is no discernible atomic volume discontinuity between the hcp and dhcp phases, the P–V–T data from the dhcp phase are also included in the determination of a P–V–T EOS. For this purpose we used the Birch–Murnaghan isothermal formalism:

$$P(V, T) = \frac{3}{2}B_{0,T}\left(\left(\frac{V_{0,T}}{V}\right)^{7/3} - \left(\frac{V_{0,T}}{V}\right)^{5/3}\right)\left(1 + \frac{3}{4}(B_{0,T}' - 4)\left(\left(\frac{V_{0,T}}{V}\right)^{2/3} - 1\right)\right), \tag{2}$$
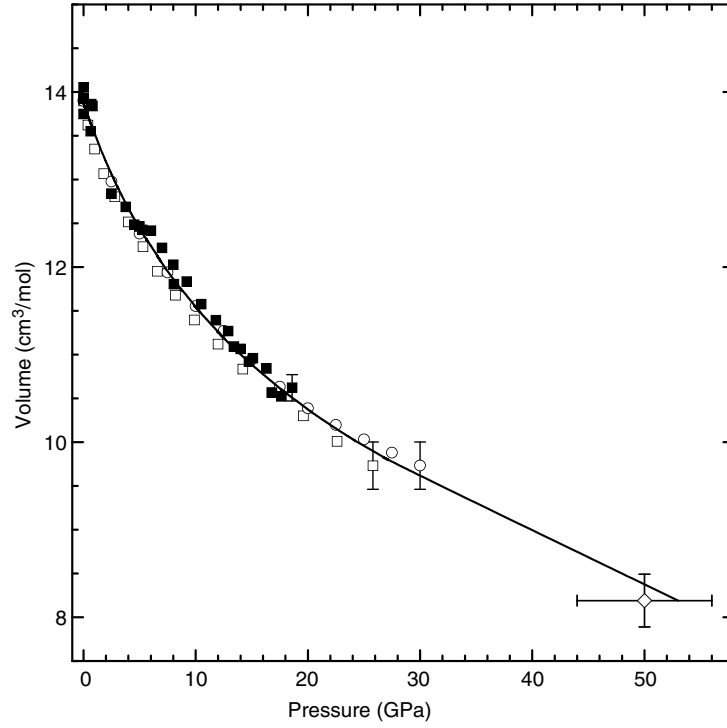
Figure 5. Compression curve of Mg at RT. (■) present data, (□) [13], (○) [14], and (◇) [12]. The solid curve represents the Birch–Murnaghan fit of all measurements, leading to $B_0 = 36.8$ GPa, with $B_0' = 4.3$ and $V_0 = 13.88$ cm^3 mol^{-1}. Typical errors for the different data sets are shown.

where

$$V_{0,T} = V_0 \exp\left(\int_{300\,\text{K}}^{T} \alpha(T)\partial T\right),$$ (3)

and

$$B_{0,T} = B_0 + \frac{\partial B_{0,T}}{\partial T}(T - 300\,\text{K}).$$ (4)

Since usually $\partial B_{0,T}/\partial T \gg \partial B_{0,T}'/\partial T$ [45], we assumed $B_{0,T}' = B_0'$. This approximation has been proved to be valid in other alkaline-earth metals like Ca, Sr, and Ba [46]. In addition, a linear behaviour of the thermal expansion coefficient was assumed, with $\alpha = \alpha_0 + (\partial\alpha/\partial T)(T - 300\,\text{K})$, where $\alpha_0 = 25 \times 10^{-6}$ K^{-1} is the thermal expansion at 300 K [47]. With these assumptions, $\partial\alpha/\partial T$ and $\partial B_{0,T}/\partial T$ are the only two parameters to be determined. By fixing $B_0 = 36.8$ GPa, $B_0' = 4.3$ and $V_0 = 13.88$ cm^3 mol^{-1} we obtained $\partial\alpha/\partial T = (2.3 \pm 0.2) \times 10^{-7}$ K^{-2} and $\partial B_{0,T}/\partial T = (-2.08 \pm 0.09) \times 10^{-2}$ GPa K^{-1}. These values compare well with those estimated in other alkaline-earth metals [46] and indicate a decrease of the bulk modulus and an increase of the thermal expansion with temperature.

4. Summary

In summary, our x-ray diffraction study of Mg does not show any evidence of the occurrence of an hcp to bcc transition in the P–T range of the present investigation. On the contrary, we
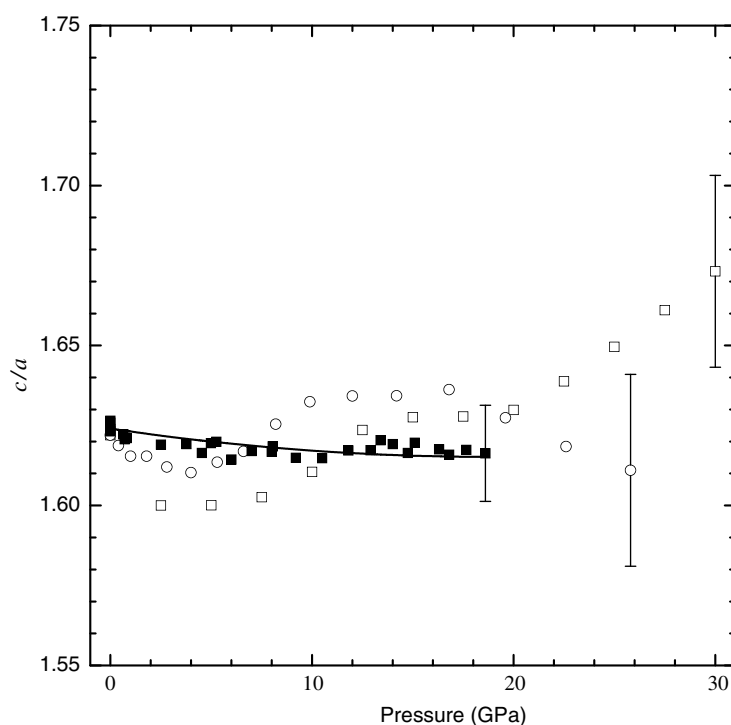
Figure 6. Axial ratio (c/a) of Mg at RT under pressure. (■) Present data, (□) [13] and (○) [14]. The full curve is the fit to our data. Typical errors for the different data sets are shown.

observed an hcp to dhcp transformation at high temperatures above 7.5 GPa. The temperature at which the hcp $\rightarrow$ dhcp transition takes place decreases as pressure increases. We also found that the hcp structure of Mg remains ideal at RT up to 18.6 GPa, which is inconsistent with the previously reported anomaly of the pressure dependence of the c/a ratio.

A P–V–T EOS was determined using the present and previous data. The parameters of this EOS are $B_0 = (36.8 \pm 3)$ GPa, $B_0' = 4.3 \pm 0.4$, $V_0 = (13.88 \pm 0.09)$ cm^3 mol^{-1}, $\alpha_0 = 25 \times 10^{-6}$ K^{-1}, $\partial\alpha/\partial T = (2.3 \pm 0.2) \times 10^{-7}$ K^{-2}, and $\partial B_{0,T}/\partial T = (-2.08 \pm 0.09) \times 10^{-2}$ GPa K^{-1}.

Acknowledgments

References

[1] Kittel C 1996 *Introduction to Solid State Physics* (New York: Wiley)
[2] Young D A 1990 *Phase Diagram of the Elements* (Berkeley, CA: University of California Press)
[3] 1996 *Crystal Structures and Lattice Parameters: Binary Alloys Phase Diagrams* 2nd edn (Materials Park, OH: ASM International)
[4] Häussermann U and Simak S I 2001 *Phys. Rev.* B **64** 245114
[5] Moriarty J A and McMahan A K 1982 *Phys. Rev. Lett.* **48** 809
[6] McMahan A K and Moriarty J A 1983 *Phys. Rev.* B **27** 3235
[7] Skriver H L 1982 *Phys. Rev. Lett.* **49** 1768

 [8] McMahan A K 1986 *Physica* B **139/140** 31
 [9] Moriarty J A and Althoff J D 1995 *Phys. Rev.* B **51** 5609
[10] Pelissier J L 1986 *Phys. Scr.* **34** 838
[11] Greef C W and Moriarty J A 1999 *Phys. Rev.* B **59** 3427
[12] Olijnyk H and Holzapfel W B 1985 *Phys. Rev.* B **31** 4682
[13] Clendenen G L and Drickamer H G 1964 *Phys. Rev.* **135** A1643
[14] Perez-Albuerne E A, Clendemen R L, Lynch R W and Drickamer H G 1966 *Phys. Rev.* **142** 392
[15] Kennedy G C and Newton R C 1963 *Solids Under Pressure* (New York: McGraw-Hill)
[16] Urtiew P A and Grover R 1977 *J. Appl. Phys.* **48** 1122
[17] Errandonea D, Boehler R and Ross M 2002 *Phys. Rev.* B **65** 012108
[18] Olijnyk H 1999 *J. Phys.: Condens. Matter* **11** 6589
[19] Vaughan M T, Weidner D J, Ko J, Wang Y, Liu X, Yaganeh-Haeri A, Pacalo R E and Zhao Y 1998
        Rev. High-Pressure Sci. Technol. **7** 1520
[20] Hanneman R E and Strong H M 1966 *J. Appl. Phys.* **37** 612
[21] Getting I C and Kennedy G C 1970 *J. Appl. Phys.* **41** 4552
[22] Walker M J, Thibault Y, Wei K and Luth R W 1995 *Can. J. Phys.* **73** 273
[23] Anderson O L, Isaac D G and Yamamoto S 1989 *J. Appl. Phys.* **65** 1534
[24] Decker D L 1971 *J. Appl. Phys.* **42** 3239
[25] Desgreniers S and Langarec K 1994 *J. Appl. Crystallogr.* **27** 432
[26] Larson A C and Von Dreele R B 1994 *Los Alamos National Laboratory Report* LAUR 86-748
[27] LeBail A, Duroy H and Fourquet J L 1988 *Mater. Res. Bull.* **23** 447
[28] Winzenik M and Holzapfel W B 1997 *Phys. Rev.* B **55** 101
[29] McMahan A K and Young D A 1984 *Phys. Lett.* A **105** 129
[30] Gotsis H J, Papaconstantoupoulus D A and Mehl M J 2002 *Phys. Rev.* B **65** 134101
[31] Yoo C S, Sonderlind P, Moriarty J A and Cambell A J 1996 *Phys. Lett.* A **214** 65
[32] Saxena S K, Dubrovinsky L S, Häggkvist P, Cerenius Y, Shen G and Mao H K 1995 *Science* **269** 1703
[33] Yoo C S, Cynn H, Soderlind P and Iota V 2000 *Phys. Rev. Lett.* **84** 4132
[34] Grosshans W A and Holzapfel W B 1992 *Phys. Rev.* B **45** 5171
[35] This texture phenomenon is well documented in hcp metals under pressure. See for example:
        Wenk H R, Matthies S, Hemley R J, Mao H K and Shu J 2000 *Nature* **405** 1044 and references therein
[36] Boehler R, Errandonea D and Ross M 2002 *High Pressure Res.* **22** 479
[37] Errandonea D, Schwager B, Ditz R, Gessmann Ch, Boehler R and Ross M 2001 *Phys. Rev.* B **63** 132104
[38] Errandonea D, Boehler R and Ross M 2000 *Phys. Rev. Lett.* **85** 3444
[39] Errandonea D, Ross M and Boehler R 2002 High-pressure phenomena: *Proc. Int. School of Physics Enrico
        Fermi* vol CXLVII, ed R J Hemley, M Bernasconi, L Ulivi and G Chiarotti
[40] Birch F 1952 *J. Geophys. Res.* **57** 227
[41] Schulte O and Holzapfel W B 1996 *Phys. Rev.* B **53** 569
[42] Velisavljevic N, Chesnut G N, Vohra Y K, Weir S T, Malba V and Akella J 2002 *Phys. Rev.* B **65** 172107
[43] Kenichi T, Hiroshi Y, Hiroshi F and Takumi K 2002 *Phys. Rev.* B **65** 132107
[44] Pearson W B 1967 *A Handbook of Lattice Spacings and Structures of Metals and Alloys* (New York: Pergamon)
[45] Dewaele A, Fiquet G, Andrault D and Häusermann D 2000 *J. Geophys. Res.* **105** 2869
[46] Anderson M S, Swenson C A and Peterson D T 1990 *Phys. Rev.* B **41** 3329
[47] Touloukian Y S 1989 *A Physicist's Desk Reference: The Second Edition of the Physics Vademecum* ed
        H L Anderson (New York: American Institute of Physics)